Proceedings of the 2022 IEEE
International Conference on Robotics and Biomimetics
December 5-9, 2022, Xishuangbanna, China

Multi-sensor Fusion for Stiffness Estimation to Assist Legged Robot Control in Unstructured Environment

Yue Gao*[1], Huajian Wu[2] and Ming Sun[2]

***Abstract*— Legged robot is designed for more flexibility when navigating in complex unstructured environment. When the end-effectors of the robot contacting non-rigid ground, the robot sinks due to different stiffness of the ground. This presents a challenge for accurate and robust control of the upper platform. In this paper, a real-time muti-sensor fusion method Dual Parallelizable Particle Filter (DPPF) is proposed to estimate ground stiffness. DPPF utilized RGB-D camera, IMU and 3-DoF force sensors. Meanwhile, we established a ground material database and trained a real-time ground segmentation network to assist the stiffness estimation of the ground. Then the information of ground material is utilized as a prior distribution for DPPF to achieve faster stiffness estimation. The experiments on synthetic data and on six-legged robot show that DPPF has faster computing speed, fewer convergent steps than previous state estimation methods. The estimated stiffness can be utilized for legged robot impedance control, posture control and trajectory planning.**

I. Introduction

Legged robots have the potential to walk and run in complex unstructured environments [1], [2]. Hence the ability of versatile force control and active terrain adaptation are necessary to fulfill the potential for legged robots [3]. While stable locomotion on rigid ground surface is challenging, the adaptation to varying stiffness brings additional difficulties, such as robot's sinking due to surface deformation on soft terrains. In this paper, we address the challenge of real-time stiffness estimation for legged robots in unstructured environments for actively adapting to different terrains.

Stiffness estimation for unknown environment is an instance of system parameters identification. Recently, some contact stiffness estimation methods are proposed for robotic manipulators, which is demonstrated to be valuable for adaptive force tracking and stability of impedance controllers [4]. For legged robots, real-time stiffness estimation of the ground contact surface is beneficial for accurate trajectory planning and actively adapting to different terrains in unstructured environments, particularly for the soft surface.

Instead of only utilizing proprioceptive sensors such as IMU and force sensor for stiffness estimation, the exteroceptive RGB-D camera can provide some important prior knowledge to assist faster estimation. when estimating ground stiffness. For instance, when the robot walks on mud, the visual information can provide soft range stiffness prior whereas when walking on asphalt road, the higher range of stiffness. Benefiting from the development of computer vision community, many effective semantic segmentation methods are proposed [5], [6], especially some recent progresses have addressed light-weight segmentation, making it available for real-time computation on robot [7], [8]. However, semantic segmentation methods focusing on ground material properties is less studied. Therefore, it is beneficial for legged robot control and planning by creating a dataset and learning a network focusing on ground understanding.

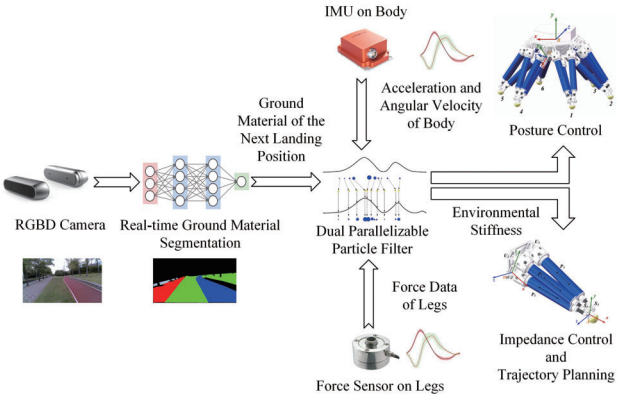

Fig. 1. Dual Parallelizable Particle Filter (DPPF) for real-time ground stiffness estimation. In each iteration, the stiffness of the next contact region is estimated by fusing data from vision, IMU and force sensors. The estimated stiffness can assist posture control, impedance control and trajectory planning for legged robots.

In this paper, ground stiffness estimation is computed to assist robot end-effector control and position control as shown in Fig. 1. The contributions of this work are the following three aspects:

- A framework for real-time stiffness estimation of ground surface for legged robot is proposed through multi-sensor fusion from vision, IMU and force sensors. A database is created to train the ground material network from images, which is utilized as the prior knowledge for stiffness estimation;
- A real-time Dual Parallelizable Particle Filter (DPPF) is proposed to estimate ground surface stiffness, which has faster computing speed and fewer convergent steps than existing methods.
- The proposed framework is demonstrated on a six-legged robot for adaptive and stable locomotion on

This work is supported by the National Key Research and Development Program of China (Grant No. 2021YFF0307900), National Natural Science Foundation of China (Grant No. 61903247), and Shanghai Municipal Science and Technology Major Project (Grant No. 2021SHZDZX0102).

[1]Yue Gao is with MoE Key Lab of Artificial Intelligence and AI Institute, Shanghai Jiao Tong University, Shanghai, P.R. China. Email: yuegao@sjtu.edu.cn

[2]Huajian Wu and Ming Sun are with Department of Automation, Shanghai Jiao Tong University, Shanghai, P.R. China. Email: {summeryuki, mingsun}@sjtu.edu.cn

*Corresponding author.

978-1-6654-8109-0/22/$31.00 © 2022 IEEE

different terrains, and the experiment results on both synthetic system and real hardware are reported.

II. Related Works

A. Legged Robot Force Control

Legged robots require versatile force control to adapt to varied terrains, which is the competitive advantage and potential over their counterparts [3]. Over the last several decades, impedance control is established for robot manipulation and legged robot force control [1], [9], [10].

To achieve steady locomotion on different surfaces, real-time stiffness and damping adjustment for impedance control is proposed for legged robot to accommodate changes in surface stiffness [11], [12], [3]. Ferris emphasized the importance of adjustable leg stiffness for the agility of legged robots [11]. Impedance modulation is proposed for impact regulation and adaptation to ground irregularity [10]. Irawan *et al.* presented an optimal impedance control scheme with adjustable parameters for hexapod robot to walk on uneven and extremely soft terrain [12].

B. State Estimation

State estimation is to compute the state of the system with noisy data according to the state and observations [13]. Kalman Filter (KF) can be utilized to estimate state for linear system with Gaussian noise [13]. For nonlinear systems, Extended Kalman Filter (EKF) is proposed to locally linearize the state or observation equations with nonlinearity. However, EKF can not be applied to highly nonlinear system, hence Unscented Kalman Filter (UKF) and Iterated Extended Kalman Filter are proposed to improve the state estimation accuracy of highly nonlinear system [14], [15].

When the measurement noise is non-Gaussian, Particle Filter (PF) can compute the posterior probability of the system by sampling a set of weighted particles based on Monte-Carlo methods [14]. The advantages of PF in nonlinear and non-Gaussian systems enable its wide applications [16]. Furthermore, dual estimation methods are preferred for systems with unknown parameters, for instance Dual Extended Kalman Filter (DEKF) and Dual Particle Filter (DPF) can be utilized to estimate parameters and state at the same time [17], [18].

C. Semantic Segmentation and Sensor Fusion with Vision

Recently, some light-weight semantic segmentation algorithms are proposed [7], [8], making it available for real-time computation on robotic platforms. For instance, BiSeNet is proposed to balance between computation speed and segmentation performance [8].

Sensor fusion with visual information can enhance the precision in some cases, which is widely applied in object tracking [19], vehicle localization [20], etc. However, sensor fusion with vision can be challenging due to its high dimensionality. One approach is to compute auxiliary information with explicit interpretations from raw visual information. Then EKF or PF can be utilized to fuse the information of other sensors with the auxiliary information from vision [21]. The alternative is to apply end-to-end learning methods which showed competitive performance in controlled environments [22]. However, end-to-end learning methods are not suitable for online stiffness estimation in unknown unseen environment.

III. System Overview

A. Robot Overview

A six-legged robot with Parallel-Parallel mechanism used in this paper is shown in Fig. 1 [23]. Each leg of the robot is designed as a 3-DoF parallel mechanism with three chains, which greatly improves the bearing capacity, stiffness and control precision. The legs are controlled through the position of end-effectors with respect to the body. The robot is equipped with a RGB-D camera, an IMU on the upper platform and one 3-DoF force sensor on the end-effector of each leg. The control scheme communicates with the actuator of each joint at 1 kHz.

B. Leg-Ground Contact Model

In this paper, impedance control is utilized for robot force control [9]. The contact force is achieved by position control through impedance model as

$$\mathbf{M}_m(\ddot{\mathbf{x}} - \ddot{\mathbf{x}}_r) + \mathbf{D}_m(\dot{\mathbf{x}} - \dot{\mathbf{x}}_r) + \mathbf{K}_m(\mathbf{x} - \mathbf{x}_r) = \mathbf{f}_d - \mathbf{f} \quad (1)$$

where $\mathbf{M}_m$, $\mathbf{D}_m$, $\mathbf{K}_m$ are the inertia, damping, stiffness matrices of target impedance model, $\mathbf{x}$ and $\mathbf{x}_r$ are the actual trajectory and the reference trajectory of end-effector, and $\mathbf{f}_d$ and $\mathbf{f}$ are the desired and actual contact force of end-effector.

When the robot contacts with the ground surface, the contact force can be expressed as

$$\mathbf{f} = \mathbf{K}_e(\mathbf{x} - \mathbf{x}_s) \quad (2)$$

where $\mathbf{K}_e$ is the ground surface stiffness, which can be calculated using DPPF described in Section IV, and $\mathbf{x}_s$ is the ground position without deformation.

C. Robot System Model

In the remaining part of this paper, the left subscript $\mathcal{W}$, $\mathcal{B}$ and $\mathcal{L}$ represent world, body and leg coordinate system, respectively. According to the forward kinematics model of the leg, the position of the robot body denoted as $\mathbf{x}$, the end-effector position of the i-th leg $\mathbf{x}^i$ can be expressed as

$$_{\mathcal{W}}\mathbf{x}^i = {}_{\mathcal{W}}\mathbf{x} + {}^{\mathcal{W}}_{\mathcal{B}}\mathbf{R}\mathbf{x}^i \quad (3)$$

where ${}^{\mathcal{W}}_{\mathcal{B}}\mathbf{R}$ is the rotation matrix from robot's body to world coordinate system, and $\mathbf{x}^i$ is the position of i-th leg's end-effector in the body coordinate, which can be calculated with forward kinematics. According to Newmark-β method and kinematics, the system model and the observation model of the robot are expressed as

$$_{\mathcal{W}}\mathbf{x}_{t+1} = {}_{\mathcal{W}}\mathbf{x}_t + {}_{\mathcal{W}}\dot{\mathbf{x}}_t\Delta t + {}_{\mathcal{W}}\ddot{\mathbf{x}}_t\frac{\Delta t^2}{2} \quad (4)$$

$$_{\mathcal{W}}\dot{\mathbf{x}}_{t+1} = {}_{\mathcal{W}}\dot{\mathbf{x}}_t + {}_{\mathcal{W}}\ddot{\mathbf{x}}_t\Delta t \quad (5)$$

$$_{\mathcal{W}}\ddot{\mathbf{x}}_{t+1} = {}_{\mathcal{W}}\ddot{\mathbf{x}}_t \quad (6)$$

$$_{\mathcal{W}}\boldsymbol{\theta}_{t+1} = {}_{\mathcal{W}}\boldsymbol{\theta}_t + {}_{\mathcal{W}}\boldsymbol{\omega}_t\Delta t \quad (7)$$

$$ {}_{\mathcal{W}}\boldsymbol{\omega}_{t+1} = {}_{\mathcal{W}}\boldsymbol{\omega}_{t} \tag{8} $$

$$ {}_{\mathcal{W}}\mathbf{f}^{i}_{t+1} = {}_{\mathcal{W}}\mathbf{f}^{i}_{t} - \mathbf{K}^{i}_{t}{}_{\mathcal{W}}\dot{\mathbf{x}}_{k}\Delta t - \mathbf{K}^{i}_{t}{}_{\mathcal{W}}\ddot{\mathbf{x}}_{t}\frac{\Delta t^2}{2} + \mathbf{K}^{i}_{t}({}_{\mathcal{B}}\mathbf{x}^{i}_{t} - {}_{\mathcal{B}}\mathbf{x}^{i}_{t+1}) \tag{9} $$

$$ \begin{pmatrix} {}_{\mathcal{W}}\ddot{\mathbf{x}}_{t} \\ {}_{\mathcal{W}}\boldsymbol{\omega}_{t} \\ {}_{\mathcal{W}}\mathbf{f}^{i}_{t} \end{pmatrix} = \begin{pmatrix} \mathbf{0} & \mathbf{0} & \mathbf{1} & \mathbf{0} & \mathbf{0} & \mathbf{0} \\ \mathbf{0} & \mathbf{0} & \mathbf{0} & \mathbf{0} & \mathbf{1} & \mathbf{0} \\ \mathbf{0} & \mathbf{0} & \mathbf{0} & \mathbf{0} & \mathbf{0} & \mathbf{1} \end{pmatrix} \begin{pmatrix} {}_{\mathcal{W}}\mathbf{x}_{t} \\ {}_{\mathcal{W}}\dot{\mathbf{x}}_{t} \\ {}_{\mathcal{W}}\ddot{\mathbf{x}}_{t} \\ {}_{\mathcal{W}}\boldsymbol{\theta}_{t} \\ {}_{\mathcal{W}}\boldsymbol{\omega}_{t} \\ {}_{\mathcal{W}}\mathbf{f}^{i}_{t} \end{pmatrix} \tag{10} $$

where $\mathbf{K}^{i}_{t}$ is the stiffness matrix of ground surface at the foothold of the i-th leg at time t, and $\mathbf{f}^{i}_{t}$ is the contact force. The robot's acceleration ${}_{\mathcal{W}}\ddot{\mathbf{x}}_{t}$ and angular velocity ${}_{\mathcal{W}}\boldsymbol{\omega}_{t}$ are estimated through IMU measurements and robot kinematics and transformed into world coordinate. 3-DoF force sensors are utilized to measure contact force at each leg and the measurements are transformed to the world coordinate. Eq. (9) represents the force generated by surface deformation due to robot's passive sinking and leg's active extension, deriving from the ground contact force model in Eq. (2).

D. Sensor Measurement Model

RGB-D camera is mounted at the center of robot's body. IMU is installed in the geometric center of the robot body. The measurement model of IMU can be represented as

$$ {}_{\mathcal{B}}\widetilde{\boldsymbol{\omega}} = {}_{\mathcal{B}}\boldsymbol{\omega} + \mathbf{b}_{w} + \mathbf{n}_{w} \tag{11} $$

$$ {}_{\mathcal{B}}\widetilde{\mathbf{a}} = {}_{\mathcal{B}}\mathbf{a} - \mathbf{g} + \mathbf{b}_{a} + \mathbf{n}_{a} \tag{12} $$

where ${}_{\mathcal{B}}\widetilde{\boldsymbol{\omega}}$ and ${}_{\mathcal{B}}\widetilde{\mathbf{a}}$ are the angular velocity and linear acceleration measurements of IMU, ${}_{\mathcal{B}}\boldsymbol{\omega}$ and ${}_{\mathcal{B}}\mathbf{a}$ are the corresponding actual values, $\mathbf{g}$ is the acceleration of gravity, $\mathbf{b}_{w}$, $\mathbf{b}_{a}$ are the measurement bias, and $\mathbf{n}_{w}$, $\mathbf{n}_{a}$ are the measurement noise.

3-DoF force sensor is mounted at the end of each leg, which measures the contact force between foot and ground

$$ {}_{\mathcal{L}}\widetilde{\mathbf{f}}_{i} = {}_{\mathcal{L}}\mathbf{f}_{i} + \mathbf{b}_{f_i} + \mathbf{n}_{f_i} \tag{13} $$

where ${}_{\mathcal{L}}\widetilde{\mathbf{f}}_{i}$ is the contact force measurement for the i_{th} leg in the leg end-effector coordinate frame, ${}_{\mathcal{L}}\mathbf{f}_{i}$ is the corresponding actual value, $\mathbf{b}_{f_i}$ is the measurement bias, and $\mathbf{n}_{f_i}$ is the measurement noise.

IV. Real-Time Stiffness Estimation

In this section, a multi-sensor based Dual Parallelizable Particle Filter (DPPF) is proposed to estimate ground stiffness in real-time, as shown in Fig. 1. During the robot's walking, BiSeNet is utilized for real-time ground material segmentation using the perceived image. The landing region of next step in the image can be computed according to the planned step size and depth image. The input of DPPF includes the stiffness range of the next landing region and the information from IMU and force sensors. When the robot legs start to touch the ground, DPPF identifies the stiffness $\hat{k}$. The estimated stiffness can be utilized for posture control and leg trajectory compensation. At the same time, impedance control maintains the contact force and trajectory planning of the robot's legs enables the smooth walking trajectory when traversing different ground materials.

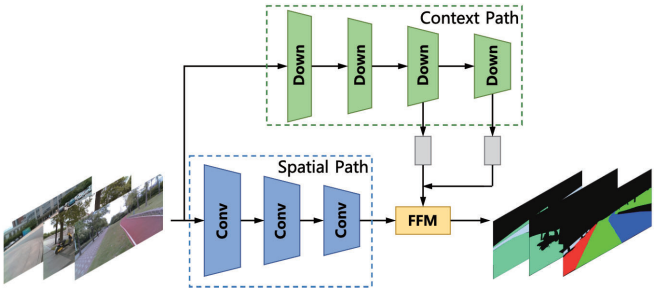

Fig. 2. Ground material segmentation database and network. The database contains 300 images with 11 categories of ground materials. The spatial path is shown as blue blocks and the context path is shown as green blocks.

A. Real-Time Ground Material Segmentation

For real-time ground material segmentation, a ground material database is created as shown in Fig. 2, which contains 300 images with 11 categories of different ground materials, including grass, mud, sand, wood, plastic road, asphalt, sponge, water, ceramic tile, foam and brick. The images are manually annotated at pixel level to train the segmentation model, which is then implemented on the onboard computer of the robot for real-time segmentation.

In this paper, BiSeNet is utilized for real-time ground material segmentation [8]. BiSeNet consists of spatial path with a small stride for spatial information preservation and context path with global average pooling for large receptive field offering. Specifically, the spatial path is comprised of three convolution layers with stride and the context path utilizes the pre-trained Xception model as backbone [24], as shown in Fig. 2.

The following joint loss L is utilized to optimize the model

$$ L(X, \hat{X}; \Theta) = l_{p}(X, \hat{X}; \Theta) + \alpha \sum_{i=2}^{k} l_{i}(X_{i}, \hat{X}_{i}; \Theta) \tag{14} $$

where X is the predicted semantic label map, $\hat{X}$ is the ground truth label, Θ is the weight of the model. l_{p} represents the principal loss function for the whole network, and l_{i} is the auxiliary loss function to supervise Context Path and i represents the stage of Xception. Softmax loss represented is utilized for all the loss functions. α is a hyper-parameter to balance principal and auxiliary loss functions. As suggested in [8], K is selected as 3 in this paper.

B. Dual Parallelizable Particle Filter

Dual Particle Filter (DPF) estimates states and unknown parameters in the model with two set of particle filters. To improve real-time performance of the stiffness estimator, multi-sensor fusion based Dual Parallelizable Particle Filter (DPPF) is proposed, which is shown in Algorithm 1. In DPPF, the two particle filters are independent of each other, hence the computation can be performed in parallel.

Algorithm 1: Multi-Sensor Fusion for Stiffness Estimation with DPPF

Load the ground material segmentation model $\mathcal{G}$.
Randomly generate N state particles x_0^i and the importance weights are set to $1/N$.
Randomly generate N parameter particles θ_0^i on the basis of the probability density function $f(\theta;\alpha,\beta)$ where $\alpha=\alpha_0^i$ and $\beta=\beta_0^i$.
Define h as the smoothing parameter with $h>0$.
Compute ground material segmentation g using RGB image o: $g=\mathcal{G}(o)$.
Calculate the region of next foothold f based on RGBD image.
Compute the probability distribution for the region f and obtain the stiffness range (r_l, r_u).
for $t=1:\infty$ **do**
  for $i=1:N$ **do**
    $\xi_t^i=\theta_t^i(r_u-r_l)+r_l$
    Importance sampling:
    $w_{t,x}^i \propto \dfrac{p(y_t|\hat{x}_t^i,\xi_{t-1})p(\hat{x}_t^i|x_{t-1}^i,\xi_{t-1})}{q_x(\hat{x}_t^i|x_{0:t}^i,y_{1:t},\xi_{t-1})}$
    Importance sampling:
    $w_{t,\xi}^i \propto \dfrac{f(\theta;\alpha_t^i,\beta_t^i)p(y_t|\xi_t^i,x_t)}{q_\xi(\xi_t^i|y_{1:t})}$
    Importance sampling: $w_t^i=w_{t,x}^i * w_{t,\xi}^i$
    Normalized $\tilde{w}_t^i=w_t^i/\sum_{j=1}^N w_t^i$
    Resampling: If $1/\sum_{i=1}^N(\tilde{w}_t^i)^2 \le N$ resample to obtain new state particles $x_{0:t}^i, i=1,2...,N$ and the importance weight are set to $1/N$.
    The state estimation is $x_t=\sum_{i=1}^N \tilde{w}_t^i x_t^i$.
    The parameter estimation is $\hat{\xi}_t=\sum_{i=1}^{N_\xi}\tilde{w}_t^i\xi_t^i$.
    The parameter variance is $\sigma_\xi^2=\sum_{i=1}^{N_\xi}(\xi_t^i-\hat{\xi}_k)^2\tilde{w}_t^i$.
    Update the parameters of the $\alpha-\beta$ distribution:
    $m_t^i=\sqrt{1-h^2}\xi_t^i+(1-\sqrt{1-h^2})\hat{\xi}_t$
    $\mu_t^i=\dfrac{m_t^i-r_l}{r_u-r_l}$
    ${\sigma_t^i}^2=\dfrac{h^2\sigma_\xi^2}{(r_u-r_l)^2}$
    $\alpha_t^i=\dfrac{{\mu_t^i}^2(1-\mu_t^i)}{{\sigma_t^i}^2}-\mu_t^i$
    $\beta_t^i=(\dfrac{{\mu_t^i}^2(1-\mu_t^i)}{{\sigma_t^i}^2})(1-\mu_t^i)$
  end for
end for

During one step of a gait, the ground surface stiffness is considered as a constant. Alpha-beta distribution is utilized as the prior knowledge from the visual information. Then the parameters are updated iteratively. In this paper, the prior knowledge of the range of ground surface stiffness is denoted as (r_l, r_u). In each step, the stiffness range (r_l, r_u) is obtained through ground material segmentation and according to the index provided by the ground label

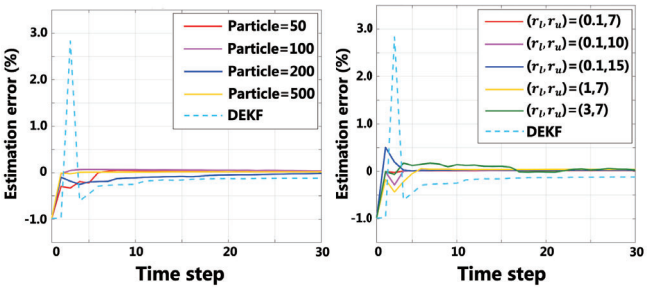

Fig. 3. Experiment results on synthetic system of DEKF and DPPF, with different number of particles and different priors of unknown parameter.

type, stiffness range can be looked up in the pre-defined database.If the ground material type has never seen before, a default large enough range is provided.

Considering the model in the form of

$$\mathbf{x}_{k+1}=\mathbf{F}(\mathbf{x}_k,\mathbf{u}_k,\xi)+\mathbf{r}_k \tag{15}$$

$$\mathbf{y}_k=\mathbf{C}\mathbf{x}_k+\mathbf{v}_k \tag{16}$$

where $\mathbf{r}_k$ and $\mathbf{v}_k$ represent the process noise and the measurement noise. $\mathbf{y}_k$ is the observation and ξ is the parameter to be identified. The prior knowledge of ξ follows the alpha-beta distribution with parameter (α,β), where probability density function can be expressed as

$$f(\theta;\alpha,\beta)=\begin{cases}\frac{1}{B(\alpha,\beta)}\theta^{(\alpha-1)}(1-\theta)^{(\beta-1)} & 0<\theta<1\\ 0 & others\end{cases} \tag{17}$$

$$\xi=\theta(r_u-r_l)+r_l \tag{18}$$

where (r_l, r_u) is the range of the unknown parameter ξ. The parameter estimation converges through iteratively updating the values of α and β.

V. Experiments

In this section, the experiment results of DPPF is presented on both synthetic system and stiffness estimation for six-legged robot. The reported results aim to demonstrate that DPPF has faster computing speed and fewer convergence steps than the existing methods.

A. Synthetic Data

To evaluate the performance of the proposed method, DPPF is used on a discrete Single-Input Single-Output system with unknown parameter

$$x_{t+1}=0.5x_t+25k\frac{x_t}{1+x_t^2}+8cos(1.2(t-1)) \tag{19}$$

$$y_t=0.05x_t^2 \tag{20}$$

where k is the unknown parameter. The covariance of process noise and measurement noise are set to $Q=1$ and $R=1$.

The results of DPPF comparing with DPF and DEKF are shown in Fig. 3. The solid lines represent results of DPPF with different number of particles, and the dotted lines represent results of DEKF. DPPF outperforms DEKF in terms

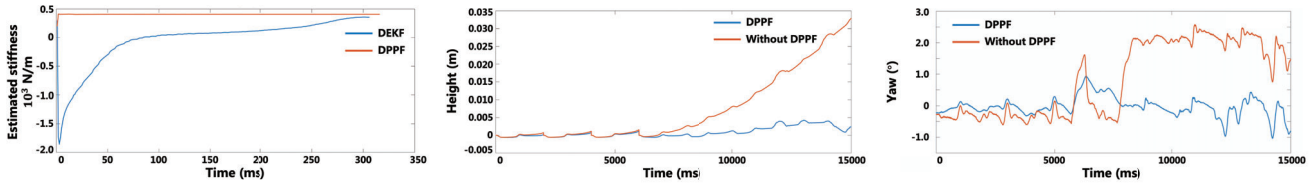

(a) (b) (c)

Fig. 4. Experiment results on six-legged robot. (a) Stiffness estimation results of DPPF and DEKF for one step on soft terrain. (b) and (c) Trajectories of height and angle during 3-3 gait traversing two different terrains.

TABLE I
COMPARISON BETWEEN DPPF, DPF AND DEKF

	# of Particles	RMSE after 100 Iterations	Time Cost for One Iteration
DPPF	5000	0.1297	0.1905 s
	500	0.6478	0.0189 s
	200	3.3134	0.0130 s
	100	7.5134	0.0080 s
DPF	5000	0.3604	0.7041 s
	500	0.5011	0.0698 s
	200	3.8343	0.0499 s
	100	6.3127	0.0130 s
DEKF	/	6.9178	0.0070 s

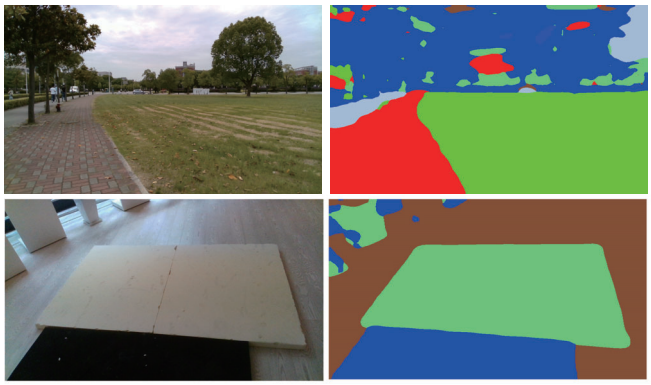

Fig. 5. Ground material segmentation results of the trained BiSeNet. Each category of material corresponds to a stiffness range, which is used as the prior for DPPF.

of the rate of convergence with less oscillations. Meanwhile, the convergence of parameter estimation accelerates as the number of particles increases.

TABLE I shows the comparisons between DPPF and baseline methods. Root-Mean-Square Errors (RMSE) of state x is reported after 100 iterations. The results demonstrate that DPPF achieves more accurate estimation comparing with DPF and DEKF on the nonlinear system expressed in Eq. (19) and (20). Compared with DPF, DPPF costs much less time comparing with DPF due to its parallel computation, especially for large number of particles. DEKF takes less computational time than DPPF in this SISO system, but it may cost more time in than DPPF for the system with high-dimensionality.

B. Real-Time Ground Material Segmentation Network

The 300 images in ground material dataset are split into 250 images for training and 50 images for validation. The segmentation computation is up to 70 FPS on the robot platform and the result of ground material segmentation is shown in Fig. 5, which meets the requirements in real-time performance and accuracy for stiffness estimation.

C. Compensation on Soft Terrain

In this experiment, the robot takes one step on the sponge surface and compensates for sinking to maintain the height of body through the estimated stiffness. The stiffness estimation results of DEKF and DPPF are shown as Fig. 4(a). The prior stiffness range from visual information of DPPF is $(r_l, r_u) = (0.1, 0.7)$. DPPF and DEKF converge to a similar value, but DPPF takes significantly less time for convergence comparing with DEKF.

TABLE II shows the comparison results between DPPF, DPF with prior knowledge from vision and DEKF without prior knowledge. Comparing with DPF and DEKF, DPPF showcases the advantages in convergence and computational time-cost due to its parallel computation. With the prior knowledge from visual information, DPPF can quickly estimate the ground stiffness and adjust body position and posture to keep the body stable and reduce the oscillation.

D. Walking Compensation on Different Terrains

To validate the effectiveness of DPPF in stiffness estimation for gait adaptation, the robot traverses two different terrains by a 3-3 gait, while maintaining the contact force and body posture to accommodate changes in surface stiffness. As shown in Fig. 6, the robot traverses from the black, soft sponge to the yellow, hard foam with same thickness.

During the robot's walking, the trained BiSeNet is used for ground material segmentation, as shown in Fig. 5. The prior knowledge is provided for DPPF to estimate ground stiffness, which is then used to compute the compensation for sinking. Fig. 4(b) and 4(c) shows the trajectories of height and posture during walking with/without stiffness estimation using DPPF. The oscillation range of height and posture is less than $0.003\ m$, $0.5°$ with DPPF, while up to $0.030\ m$, $2.5°$ without DPPF.

Fig. 6. The robot traverses from the black, soft sponge to the yellow, hard foam by a 3-3 gait. DPPF with the prior from ground material segmentation is utilized for real-time stiffness estimation. With the estimated stiffness, the contact force can be maintained more accurately and the robot's body relative to the ground can be kept with a constant height and posture.

TABLE II
COMPARISON OF STIFFNESS ESTIMATION RESULTS BETWEEN DPPF WITH VISION, DPF WITH VISION AND DEKF WITHOUT VISION

Algorithm	Estimated Sinking Depth	Converge Iteration	Time Cost for One Iteration
DPPF w/ Vision	0.036 m	30	0.008 s
DPF w/ Vision	0.036 m	27	0.180 s
DEKF w/o Vision	0.033 m	300	0.074 s
Ground Truth	0.035 m	/	/

VI. CONCLUSIONS

Legged robot real-time stiffness estimation is crucial for legged robot planning and control in unstructured environment. Dual Parallelizable Particle Filter is proposed in this paper for real-time stiffness estimation by fusing RGBD camera, IMU and 3-DoF force sensor, which has much faster computing speed and fewer convergent steps. Furthermore, a ground material database is created to train the real-time ground material segmentation network. The estimated stiffness using DPPF can be utilized for real-time posture control, force control and trajectory planning.

REFERENCES

[1] J. Park and J. H. Park, "Impedance control of quadruped robot and its impedance characteristic modulation for trotting on irregular terrain," in *2012 IEEE/RSJ International Conference on Intelligent Robots and Systems*. IEEE, 2012, pp. 175–180.

[2] J. Lee, J. Hwangbo, L. Wellhausen, V. Koltun, and M. Hutter, "Learning quadrupedal locomotion over challenging terrain," *Science robotics*, vol. 5, no. 47, 2020.

[3] C. Semini, V. Barasuol, T. Boaventura, M. Frigerio, M. Focchi, D. G. Caldwell, and J. Buchli, "Towards versatile legged robots through active impedance control," *The International Journal of Robotics Research*, vol. 34, no. 7, pp. 1003–1020, 2015.

[4] D. Erickson, M. Weber, and I. Sharf, "Contact stiffness and damping estimation for robotic systems," *The International Journal of Robotics Research*, vol. 22, no. 1, pp. 41–57, 2003.

[5] J. Long, E. Shelhamer, and T. Darrell, "Fully convolutional networks for semantic segmentation," in *Proceedings of the IEEE conference on computer vision and pattern recognition*, 2015, pp. 3431–3440.

[6] H. Noh, S. Hong, and B. Han, "Learning deconvolution network for semantic segmentation," in *Proceedings of the IEEE international conference on computer vision*, 2015, pp. 1520–1528.

[7] E. Romera, J. M. Alvarez, L. M. Bergasa, and R. Arroyo, "Erfnet: Efficient residual factorized convnet for real-time semantic segmentation," *IEEE Transactions on Intelligent Transportation Systems*, vol. 19, no. 1, pp. 263–272, 2017.

[8] C. Yu, J. Wang, C. Peng, C. Gao, G. Yu, and N. Sang, "Bisenet: Bilateral segmentation network for real-time semantic segmentation," in *Proceedings of the European Conference on Computer Vision (ECCV)*, 2018, pp. 325–341.

[9] N. Hogan, "Impedance control: An approach to manipulation," in *1984 American control conference*. IEEE, 1984, pp. 304–313.

[10] J. H. Park, "Impedance control for biped robot locomotion," *IEEE Transactions on Robotics and Automation*, vol. 17, no. 6, pp. 870–882, 2001.

[11] D. P. Ferris, M. Louie, and C. T. Farley, "Running in the real world: adjusting leg stiffness for different surfaces," *Proceedings of the Royal Society of London. Series B: Biological Sciences*, vol. 265, no. 1400, pp. 989–994, 1998.

[12] A. Irawan and K. Nonami, "Optimal impedance control based on body inertia for a hydraulically driven hexapod robot walking on uneven and extremely soft terrain," *Journal of Field Robotics*, vol. 28, no. 5, pp. 690–713, 2011.

[13] T. D. Barfoot, *State Estimation for Robotics*. Cambridge University Press, 2017.

[14] R. Van Der Merwe, A. Doucet, N. De Freitas, and E. A. Wan, "The unscented particle filter," in *Advances in neural information processing systems*, 2001, pp. 584–590.

[15] J. Zhao, M. Netto, and L. Mili, "A robust iterated extended kalman filter for power system dynamic state estimation," *IEEE Transactions on Power Systems*, vol. 32, no. 4, pp. 3205–3216, 2016.

[16] J. González, J.-L. Blanco, C. Galindo, A. Ortiz-de Galisteo, J.-A. Fernández-Madrigal, F. A. Moreno, and J. L. Martinez, "Mobile robot localization based on ultra-wide-band ranging: A particle filter approach," *Robotics and Autonomous Systems*, vol. 57, no. 5, pp. 496–507, 2009.

[17] E. A. Wan and A. T. Nelson, "Dual extended kalman filter methods," *Kalman filtering and neural networks*, vol. 123, 2001.

[18] L. E. Olivier, B. Huang, and I. K. Craig, "Dual particle filters for state and parameter estimation with application to a run-of-mine ore mill," *Journal of Process Control*, vol. 22, no. 4, pp. 710–717, 2012.

[19] H. Cho, Y.-W. Seo, B. V. Kumar, and R. R. Rajkumar, "A multi-sensor fusion system for moving object detection and tracking in urban driving environments," in *2014 IEEE International Conference on Robotics and Automation (ICRA)*. IEEE, 2014, pp. 1836–1843.

[20] G. Wan, X. Yang, R. Cai, H. Li, Y. Zhou, H. Wang, and S. Song, "Robust and precise vehicle localization based on multi-sensor fusion in diverse city scenes," in *2018 IEEE International Conference on Robotics and Automation (ICRA)*. IEEE, 2018, pp. 4670–4677.

[21] A. Martinelli and A. Renzaglia, "Cooperative visual-inertial sensor fusion: Fundamental equations," in *2017 International Symposium on Multi-Robot and Multi-Agent Systems (MRS)*. IEEE, 2017, pp. 24–31.

[22] M. A. Lee, Y. Zhu, K. Srinivasan, P. Shah, S. Savarese, L. Fei-Fei, A. Garg, and J. Bohg, "Making sense of vision and touch: Self-supervised learning of multimodal representations for contact-rich tasks," in *2019 International Conference on Robotics and Automation (ICRA)*. IEEE, 2019, pp. 8943–8950.

[23] Y. Pan and F. Gao, "A new six-parallel-legged walking robot for drilling holes on the fuselage," *Proceedings of the Institution of Mechanical Engineers, Part C: Journal of Mechanical Engineering Science*, vol. 228, no. 4, pp. 753–764, 2014.

[24] F. Chollet, "Xception: Deep learning with depthwise separable convolutions," in *Proceedings of the IEEE conference on computer vision and pattern recognition*, 2017, pp. 1251–1258.